◆ Human Brain Mapping 36:549–565 (2015) ◆

Spatial and Temporal Functional Connectivity Changes Between Resting and Attentive States

Signe Bray,[1,2,3,4,5]* Aiden E.G.F. Arnold,[3,4,6,7,8] Richard M. Levy,[9] and Giuseppe Iaria[3,4,6,7,8]

[1]*Department of Radiology, University of Calgary, Calgary, Alberta, Canada*
[2]*Department of Psychiatry, University of Calgary, Calgary, Alberta, Canada*
[3]*Hotchkiss Brain Institute, University of Calgary, Calgary, Alberta, Canada*
[4]*Alberta Children's Hospital Research Institute, University of Calgary, Calgary, Alberta, Canada*
[5]*Child and Adolescent Imaging Research Program, Alberta Children's Hospital, Calgary, Alberta, Canada*
[6]*Department of Psychology, University of Calgary, Calgary, Alberta, Canada*
[7]*Department of Clinical Neurosciences, University of Calgary, Calgary, Alberta, Canada*
[8]*NeuroLab, University of Calgary, Calgary, Alberta, Canada*
[9]*Faculty of Environmental Design, University of Calgary, Calgary, Alberta, Canada*

Abstract: Remote brain regions show correlated spontaneous activity at rest within well described intrinsic connectivity networks (ICNs). Meta-analytic coactivation studies have uncovered networks similar to resting ICNs, suggesting that in task states connectivity modulations may occur principally within ICNs. However, it has also been suggested that specific "hub" regions dynamically link networks under different task conditions. Here, we used functional magnetic resonance imaging at rest and a continuous visual attention task in 16 participants to investigate whether a shift from rest to attention was reflected by within-network connectivity modulation, or changes in network topography. Our analyses revealed evidence for both modulation of connectivity within the default-mode (DMN) and dorsal attention networks (DAN) between conditions, and identified a set of regions including the temporoparietal junction (TPJ) and posterior middle frontal gyrus (MFG) that switched between the DMN and DAN depending on the task. We further investigated the temporal nonstationarity of flexible (TPJ and MFG) regions during both attention and rest. This showed that moment-to-moment differences in connectivity at rest mirrored the variation in connectivity between tasks. Task-dependent changes in functional connectivity of flexible regions may, therefore, be understood as shifts in the pro-

Additional Supporting Information may be found in the online version of this article.

Contract grant sponsors: NSERC PDF, NSERC Discovery Grant and iCore, the Alberta Children's Hospital Foundation and the Sinneave Family Foundation (S.B.); Contract grant sponsors: Social Sciences and Humanities Research Council of Canada (SSHRC) (G.I.) and Natural Science and Engineering Research Council of Canada (NSERC) Discovery Grant (G.I.); Contract grant sponsors: Alberta Health Services and the Ministry of Human Services as a part of the Collaborative Research Grant Initiative: Mental Wellness in Seniors and Persons with Disabilities and an NSERC PGS D (A.A.)

*Correspondence to: Signe Bray; University of Calgary, Alberta Children's Hospital, BRU B4-517, 2888 Shaganappi Trail NW, Calgary, AB, Canada T3B 6A8. E-mail: slbray@ucalgary.ca

Received for publication 2 June 2014; Revised 16 September 2014; Accepted 22 September 2014.

DOI: 10.1002/hbm.22646
Published online 1 October 2014 in Wiley Online Library (wileyonlinelibrary.com).

portion of time specific connections are engaged, rather than a switch between networks per se. This ability of specific regions to dynamically link ICNs under different task conditions may play an important role in behavioral flexibility. *Hum Brain Mapp 36:549–565, 2015.*

Key words: resting functional magnetic resonance imaging; connectivity; networks; attention; hubs

INTRODUCTION

Activity in distant regions of the human brain shows temporally correlated low frequency oscillations, even when people are resting passively [Biswal et al., 1995]. Analysis of these inter-regional correlations has revealed several large-scale neural networks at rest [Damoiseaux et al., 2006; Fox et al., 2005; Power et al., 2011; Yeo et al., 2011]. These networks, termed resting state (RSNs) or intrinsic connectivity (ICNs) networks are supported by underlying structural connections [Greicius et al., 2009; Honey et al., 2009; van den Heuvel et al., 2009] and are thought to reflect functionally meaningful units of brain organization. Although there is variability in the number of ICNs identified in different studies, most reports have identified default mode (DMN) and dorsal attention (DAN) (also called task-positive or frontoparietal) networks, as well as visual, sensorimotor, auditory, and subcortical networks. Importantly, similar networks have been identified across multiple modalities, including electroencephalography [He et al., 2008], electrocorticography [Nir et al., 2008], and magnetoencephalography (MEG) [Betti et al., 2013; Brookes et al., 2011; de Pasquale et al., 2012; Hipp et al., 2012].

ICNs are identified from functional magnetic resonance imaging (fMRI) scans obtained when volunteers are resting and, therefore, not specifically engaging, for example, motor or attention networks. It is, therefore, interesting that the regions grouped in ICNs can typically be linked with cognitive and perceptual functions. Indeed, the regions that are linked in ICNs are also often coactivated during functional tasks, as evidenced by meta-analytic connectivity studies [Smith et al., 2009; Toro et al., 2008]. This suggests that the organization revealed by ICNs is relatively stable across task states, including rest, and that task states may modulate connectivity within and between ICNs rather than spatially reconfigure these networks. In support of this view, recent work has shown that while the dynamics of interactions within and between ICNs changes from rest to free-viewing a movie, the topography of these networks remains similar [Betti et al., 2013].

However, while somewhat segregated, communication between these networks is necessary for complex cognitive functions, and is thought to occur through network "hubs," that is, regions that interface with multiple networks [Buckner et al., 2009; Cole et al., 2010, 2013; Fox et al., 2006; de Pasquale et al., 2013; Power et al., 2013; Tomasi and Volkow, 2011]. Indeed, recent studies have suggested that some regions may show particular flexibility, shifting functional connectivity with other networks during different task states [Cole et al., 2013; Fornito et al., 2012].

Visual attention is thought to increase functional connectivity between frontal and parietal regions [Szczepanski et al., 2013], as well as between parietal and occipital [Greenberg et al., 2012] and high- and low-level visual regions [Al-Aidroos et al., 2012]. From a network perspective, it has been suggested that the structure of intrinsic and extrinsic networks is largely preserved during continuous attention tasks [Golland et al., 2008], and that while there are changes in between network connectivity, the topography of networks remains similar between natural scene viewing and rest [Betti et al., 2013]. It has also been suggested that there is an overall decrease in the density of functional connections during visual attention relative to rest [Tomasi et al., 2013].

In this study, we asked whether a change from a resting to attentive cognitive state is reflected by modulation of connectivity within ICNs, or a spatial reconfiguration of networks. To address this question we examined data collected during both rest and a spatial learning task [Arnold et al., 2014] requiring continuous visual attention. During this task participants were passively guided through a virtual city with salient landmarks and asked to learn the spatial layout. While this is not a "pure" attention task as it additionally engages object recognition and working memory processes, the learning requirement served to maintain a consistently attentive state despite the absence of overt responding during the task.

We applied a data-driven connectivity clustering analysis (e.g., [Bray et al., 2013; Lee et al., 2012; Liu et al., 2012; Wang and Li, 2013; Golland et al., 2008]) to identify a set of distributed networks, and compared the spatial extent of these networks between conditions. Our analyses showed that broadly similar networks were identified during resting and attentive states, but that several "flexible" regions near internetwork borders showed preferential connectivity with different networks depending on the task. This was confirmed using follow-up seed-based analyses. We additionally asked whether the task modulated within-network connectivity, using seed analyses from core nodes of the DMN and DAN. Finally, as recent work suggests that even at rest there is variability in connectivity patterns across time, we used a temporal nonstationarity analysis to ask whether flexible regions showed spatial

patterns at rest that might predict between- task variability in connectivity.

METHODS

Abbreviations

Abbreviations used throughout the manuscript are listed in Supporting Information Table 1.

Participants

Sixteen healthy, right-handed volunteers (9 females, mean age 22 years, age range 18–36 years) with no history of psychiatric or neurological disorders, and normal or corrected-to-normal vision participated in the study. All participants provided written informed consent as approved by the Conjoint Health Research Ethics Board at the University of Calgary.

fMRI Tasks

Rest

During resting scans, participants were asked to fixate a small black cross on a white screen. Resting scans lasted 5 min in 9 participants and 10 min in 7 participants. For consistency across analyses, all scans were truncated to the first 5 min (120 volumes).

Continuous visual attention—spatial learning task

Participants performed a task requiring continuous visual attention while viewing a changing visual display. During this task participants were passively guided through a virtual city with specific landmarks, and were tasked with learning the layout. Spatial learning relies heavily on attention and working memory networks as well as the hippocampus [Burgess et al., 2001; Byrne et al., 2007; Hartley et al., 2003; Iaria et al., 2003; Maguire et al., 1998]. During this task, participants viewed nine 1-min video clips of random passive movement in first-person perspective through a virtual environment that included four unique landmarks in a 5 × 5 rectangular grid of identical buildings (Supporting Information Fig. 1). They additionally viewed three control clips of a virtual environment with no unique landmarks in a similar 5 × 5 rectangular grid. Experimental and control clips were presented in pseudorandom order: a control clip was presented at the start and end of the run, with nine experimental clips and one control clip presented in randomized order in between the control clips. Interstimulus intervals between 4 and 6 s were randomized between clips. All participants were given a verbal overview of the task instructions before entering the scanner. This task has been previously described in Arnold et al. [2014]. For analyses described here, time series were extracted from only the experimental clips and truncated to include only the first 120 experimental condition volumes. Thus, connectivity analyses were performed by calculating intervoxel correlations averaged over 5-min, during which visual attention was consistently required.

MR Acquisition

Participants were scanned using a 3T GE Signa scanner with an eight-channel head coil at the Seaman Family MR Research Centre at the University of Calgary. Both resting-state and task-based functional scans were acquired using a T2*-weighted EPI sequence of 45 slices (repetition time (TR) = 2,500 ms, echo time (TE) = 30 ms, FOV = 24.0 cm, 3 × 3 × 3 mm voxels in interleaved acquisition, flip angle = 77°). An additional 5 volumes were discarded from the start of each run to allow for T1 equilibration. Resting-state scans were conducted prior to task-based functional scans in all participants. High-resolution three-dimensional anatomical images were acquired using a SPGR sequence (180 slices, FOV = 25.6 cm, 1 × 1 × 1 mm voxels, flip angle = 11°). A T2-weighted fast SPGR was also acquired in the same orientation as functional runs, and was used to facilitate coregistration of functional and structural scans.

fMRI Preprocessing

Data from rest and task scans were preprocessed identically using the SPM8 (http://www.fil.ion.ucl.ac.uk/spm/software/spm8/) MATLAB (Mathworks, Natick, MA) toolbox, as well as custom MATLAB routines. All scans were slice-time corrected and realigned to the first scan acquired in each session. Functional images were coregistered to each participants' T2-weighted image, and these were in turn coregistered to the high-resolution anatomical image. Anatomical images were segmented into grey matter, white matter, and cerebral spinal fluid (CSF). To reduce physiological and motion confounds, residual functional images were obtained by regressing out the six estimated motion parameters and their temporal derivatives, as well as signal obtained by averaging over white matter and CSF voxels [Dagli et al., 1999; Van Dijk et al., 2010; Weissenbacher et al., 2009; Windischberger et al., 2002]. Global signal regression was not performed to avoid the possible introduction of confounds [Murphy et al., 2009; Saad et al., 2012]. A linear trend was subtracted from each voxel to correct for scanner drift, and all values were converted to a %-change value from the mean. ArtRepair software [Mazaika et al., 2009] was used to identify volumes in which scan-to-scan motion was greater than 0.5 mm/TR. These volumes were excluded from subsequent correlation calculations (i.e., similar to [Power et al., 2012]); between 0 and 13 volumes were excluded (mean = 2), this number was not significantly different for task and rest ($P = 1$). Images were normalized to the MNI template

using parameters obtained from the anatomical segmentation, resampled to 4 mm^3 voxels, and spatially smoothed with a 6 mm FWHM Gaussian kernel. All reported coordinates are in MNI template space. Recent work suggests that spectral information in RSNs is present not only in low-frequency components [Niazy et al., 2011], and we chose not to filter resting data to maintain consistency between processing of task and rest scans. However, results from a similar analysis using low-pass filtered resting data (0.1 Hz cutoff) showed a similar pattern (reported in Supporting Information Results).

fMRI Analyses

To investigate whether functional network topography changes between attention and rest, a series of analyses were undertaken. First, we applied a data-driven whole-brain connectivity clustering approach to ask (1) whether similar networks would be identified in the task and rest conditions and (2) whether these networks were similar in spatial extent. To be more specific, we tested the hypothesis that networks with similar core regions might expand or contract between conditions. This analysis showed that similar networks could be identified between conditions, though with key differences in spatial extent near internetwork borders; we term regions that switched between networks depending on the task "flexible."

Second, we used seed-based analyses to ask whether connectivity within canonical networks was amplified during the task relative to rest, and whether flexible regions indeed showed differential connectivity with networks between tasks.

Finally, as recent work has suggested that even within canonical ICNs there is moment-to-moment variability in spatial connectivity patterns [Liu and Duyn, 2013], we used temporal nonstationarity analyses to ask whether connectivity changes of flexible regions represent a change in the temporal allocation of connectivity between networks rather than a shift in connectivity between networks.

Spatial Clustering Analyses

A grey matter mask was obtained by averaging the normalized grey-matter images from each participant, smoothing, resampling to 4 mm^3 voxels and thresholding at 0.4. This image was masked to exclude the cerebellum and included only voxels present across all participants' functional scans, resulting in an image with 19,210 voxels. For the resting scans, time courses were obtained from the first 120 volumes in the grey matter mask. For the attention-task scans, the first 120 volumes acquired during the task condition were used to generate time courses (volumes acquired during the control condition were excluded). For each participant, and each task, a 19,210 $\times$ 19,210 correlation matrix was obtained from the Pearson correlation of the time course from each voxel with every other voxel. Clustering analyses were run first at the group level, for which connectivity matrices were averaged over all participants, within each task. To run statistical comparisons, single-subject clusters were also obtained.

Fuzzy c-means clustering, implemented in the MATLAB Fuzzy logic toolbox [Bezdec, 1981], was used to divide the connectivity matrix into clusters of similar rows. Briefly, this approach divides a matrix in which each row corresponds to a sample data point, into N clusters, by assigning a membership weight between 0 and 1 to each data point, for each cluster. The clustering algorithm iteratively updates cluster centers and the membership grades for each data point, gradually minimizing an objective function that represents the distance from any given data point to a cluster center, weighted by each data point's membership weight. We used a partition matrix exponent M of 1.2 (similar to [Lee et al., 2012]) and a Euclidian distance metric. The algorithm iterated until the improvement on successive iterations was less than 1; the algorithm was run five times and the results were averaged. Clusters in Figure 1 and Supporting Information Figure 2 are shown as membership weights. For group-level clustering, a random starting point was used, and individual subject clusters were seeded using the group-level clusters in each condition.

At the group-level, cluster numbers from 2 to 10 were tested. Two criteria were used in determining the appropriate number of clusters. First, as the purpose of this analysis was to compare network-level clusters between conditions, a heuristic criterion that clusters be uniquely matched between conditions was applied. The largest number of clusters that were uniquely matched across conditions was 6. We additionally calculated silhouette values for each point and averaged these. Silhouette values indicate how similar a point is to members of the same cluster, relative to members of other clusters [Kaufman and Rousseeuw, 1990]. For this analysis we assigned points to the cluster with which they showed maximal weighting. Average silhouette values for different cluster numbers are plotted in Supporting Information Figure 3 and show a decline for clusters greater than 6 in both conditions.

Statistical comparison of cluster extent

Clusters were matched between tasks at the group level by calculating the spatial correlation across all pairs of clusters, and matching clusters with maximal spatial correlation. For single-subject clusters, a similar approach was used to match clusters derived from each task with group clusters, and match clusters across tasks. Clusters derived from task were subtracted from rest within subjects. As these data were not normally distributed, these difference maps were analyzed at the group level using one-sample t-tests with the statistical nonparametric mapping toolbox (SnPM; [Nichols and Holmes, 2002]. Two-thousand permutations were run for each analysis, and 6 mm FWHM

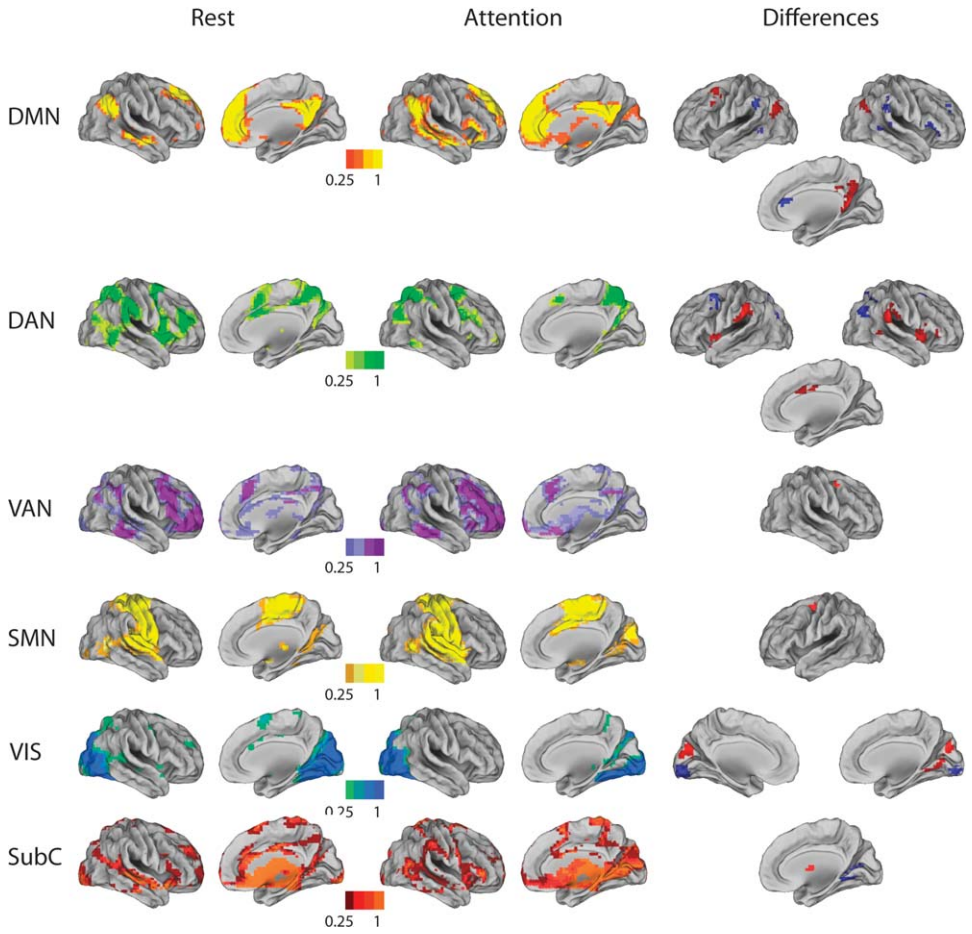

Figure 1.

Six-cluster solution. Networks derived from rest and attention conditions are shown in the left and middle columns; lateral and medial surfaces of the right hemisphere are shown. The six cluster solution identified the DMN, default mode; DAN, dorsal attention; VAN, ventral attention; SMN, supplementary motor; VIS, visual; SubC, subcortical networks. Significant differences between networks are shown in the rightmost column (left hemisphere on the left); red = rest > attention, blue = attention > rest. [Color figure can be viewed in the online issue, which is available at wileyonlinelibrary.com.]

variance smoothing was used. Inferences were drawn using family-wise error (FWE) cluster correction at $P < 0.05$ with an a priori pseudo t-value set at 3; clusters > ~20 voxels were significant at a FWE-corrected threshold.

Seed-based connectivity analyses

Two sets of seed-based connectivity analyses were conducted. The first used core regions from the DMN, DAN, and visual networks, to determine whether there was amplification of within-ICN connectivity. These regions were identified as core members of these ICNs from the previous literature, manually chosen in the region of overlap for networks defined in both conditions (see below and Supporting Information Fig. 4a,b,c). The second set of seed analyses used regions identified as flexible in the analysis comparing spatial extent of networks, to confirm that there were shifts in connectivity to the DMN and DAN between conditions (Supporting Information Fig. 4d,e). Seed regions of interest (ROIs) were generated as 3 mm radius spheres around a given voxel. Seed ROI time courses were extracted by averaging over voxels included in the ROI. For each participant, one general linear model per seed was generated in SPM8 that included both the rest and attention tasks, with the task-specific time courses from the given seed and session effects as regressors. Within-subject contrasts were generated for rest>attention and attention>rest. These contrasts were entered into random effects analyses at the second level. For flexible seeds inferences were drawn using a height threshold of $P < 0.001$ and an extent threshold FWE corrected at $P < 0.05$. For the 4 DMN and 5 DAN seeds, consistency

maps were generated to summarize the data and illustrate regions of significant difference common to multiple seeds. These maps were generated by (1) calculating thresholded binary maps for the contrast of attention > rest and rest > attention at a height of $P < 0.001$ and (2) combining these binary maps over the seeds within a network. These maps were thresholded at $P < 0.001$ uncorrected and combined; an uncorrected threshold was chosen here to highlight regions of overlap that are unlikely to be significantly different between seeds.

Temporal nonstationarity analyses

Although most resting functional connectivity studies use correlations over the duration of a scan, several recent studies have suggested that there is moment-to-moment variability in connectivity, even during rest [Chang and Glover, 2010; Liu and Duyn, 2013]. We used a temporal nonstationarity analysis to investigate whether connectivity differences between task states might be predicted from spatial connectivity patterns at rest. The temporal nonstationarity analysis followed a method similar to Liu and Duyn [2013]. These authors showed, using a modification of the point process approach [Tagliazucchi et al., 2012], that by averaging volumes corresponding to peaks in the time course of a seed region, spatial maps showing a strong resemblance to seed-correlation maps could be recovered. This suggests that averaged patterns of functional connectivity are largely driven by momentary signal peaks. They furthermore applied a temporal clustering analysis to identify different spatial modes, which they termed spontaneous coactivation patterns (CAPs). Here we applied this clustering approach to identify momentary patterns of spatial connectivity, to ask whether changes in connectivity between conditions might be suggested by varying connectivity patterns at rest.

In addition to the preprocessing steps described above, voxel time courses were mean centered and divided by their standard deviation prior to the temporal nonstationarity analysis. Time courses were extracted from seed ROIs, defined as spheres with 3 mm radius around a coordinate. For each seed region, we identified signal peaks as the top-valued 15% of temporal volumes for this seed. The volumes corresponding to these temporal peaks in each of the 16 individuals were concatenated within each task (attention and rest) separately. These volumes were entered into a k-means clustering analysis to identify consistent spatial patterns at different time points across time and participants. K-means clustering differs from fuzzy clustering in that each item is assigned to a discrete cluster. The algorithm starts by randomly assigning items to clusters, and iterating until the sum, over all clusters, of within-cluster distance to center is minimized. Our analysis used random starting points, 10 replications, and a Euclidian distance metric. For each seed, we tested 2–6 temporal clusters, and chose the highest number of clusters that indexed a spatial mode present in each of the 16 participants. We found that 2 clusters were seen consistently across subjects in the regions tested here. We present maps of the spatial average and proportion of volumes assigned to each cluster, as well as the spatial correlation between temporal clusters and group-level seed connectivity results during attention and rest. Follow-up analyses merged both tasks into a single clustering analysism, to ask whether there were differences in the temporal allocation of specific CAPs across conditions.

RESULTS

Whole Brain Connectivity Clustering

Cluster solutions resulting in 2–9 ICNs were tested. The six-cluster solution was the highest number that could be uniquely paired between conditions. Additionally, in both conditions, silhouette plots (Supporting Information Fig. 3) showed decreased values for cluster solutions greater than 6. Clusters identified from both the attention and rest connectivity matrices were recognizable based on the previous ICN literature. These networks include the DMN, DAN, ventral attention network (VAN), visual, supplementary motor, and subcortical networks [Power et al., 2011] (Fig. 1). There were, however, significant differences in the spatial extent of these networks, with the greatest differences occurring in the DMN and DAN (Fig. 1 rightmost column; Table I). Regions such as the posterior middle frontal gyrus (MFG) and superior/inferior parietal lobule (SPL/IPL) shifted from the DMN to the DAN under the task condition, relative to rest, while the temporoparietal junction (TPJ), portions of the cingulate and anterior insula shifted from the DAN to the DMN. Changes in the visual network were also observed along the parieto-occipital fissure, and in ventral visual regions. Moving from a 6- to 7-cluster solution, the networks could no longer be uniquely matched between conditions (Supporting Information Fig. 2), however, similar differences in extent were found between the DMN and DAN networks (Supporting Information Table 2).

Regions that showed significant differences between task and rest were combined across the six-cluster models and are shown in Figure 2. This map shows broad similarities to the community density map recently reported by Power et al. [2013], lending support to the hypothesis that articulation points where multiple networks intersect are probable locations for network hubs. Table I and Figure 2 are replicated in Supporting Information Results using a low-pass filter on the RSN data (Supporting Information Table 3; Supporting Information Fig. 5), which produced similar results.

Connectivity Changes with Core DMN, DAN, and Visual Network Regions

In addition to assessing differences in the spatial extent of networks, seed-based analyses were used to ask

TABLE I. Voxel-wise differences in networks between tasks

		Condition								
		Rest > Attention					Attention > Rest			
Network	Region	BA	Peak *XYZ* (mm)	Size	Peak *P*-uncorr	Region	BA	Peak *XYZ* mm	Size	Peak *P*-uncorr
DMN	Left IPS /IPL	19/7 /39	−38 −72 30	96	0.0002	Right SFG	10	18 52 22	21	0.0002
	Right IPL	19/7 /39	46 −68 34	67	0.0002	Anterior cingulate	24	6 32 14	30	0.0002
	Left MFG	6	−34 12 58	59	0.0002	Right IFG	11	54 24 2	44	0.0002
	Cuneus / Precuneus	31	10 −56 18	277	0.0002	Left temporooccipital	21	−62 −56 −6	39	0.0002
						Left TPJ	40	−58 −44 38	27	0.0002
						Right TPJ	40	66 −32 30	81	0.0002
DAN	Right TPJ	40	66 −32 30	177	0.0002	Left IPS / SPL	19/7 /39	−38 −60 34	122	0.0002
	Left TPJ	40	−66 −36 26	120	0.0002	Right IPS / SPL	19/7 /39	38 −72 38	156	0.0002
	Right anterior insula	13	58 12 2	188	0.0002	Right MFG	6	30 12 62	32	0.0002
	Left anterior insula	13	−38 0 −2	95	0.0002	Left MFG	6	−30 12 50	91	0.0002
	Cingulate	31	2 −4 38	68	0.0002					
VAN	Right MFG	6	34 8 50	23	0.001	n/a				
Motor	Left MFG	6	−22 −4 58	26	0.0002	n/a				
Subcortical	Pallidum		−2 −4 6	66	0.0002	Cerebellum / ventral visual		18 −52 −10	155	0.0002
Visual	Bilateral pericalcarine / Cuneus	18	−6 −76 22	217	0.0002	Bilateral ventral visual	17	−10 −92 −10	251	0.0002
						Right occipitotemporal	19	50 −72 18	37	0.0002

DMN, default mode network; DAN, dorsal attention network; VAN, ventral attention network; IPS, intraparietal sulcus; IPL, inferior parietal lobule; SPL, superior parietal lobule; SFG, superior frontal gyrus; MFG, middle frontal gyrus; IFG, inferior frontal gyrus; TPJ, temporoparietal junction.

whether connectivity with core nodes of the DMN, DAN and visual networks would show within-network connectivity differences between tasks. A set of four seed regions typically associated with the DMN and that were in the region of overlap for the DMN cluster in both the rest and attention tasks, were manually chosen for seed-based connectivity analyses. These included the posterior cingulate cortex (PCC) [2 −48 28], medial prefrontal cortex (mPFC) [2 56 12], and bilateral IPL [−50 −62 34], [54 −56 34] (Supporting Information Fig. 4a). Models compared connectivity patterns with these seed regions across tasks. Consistency maps indicating regions of significant difference for rest versus attention, for 1–4 DMN seeds, are shown in Figure 3a (upper panel). In rest > attention, the DMN seeds generally showed greater connectivity with several DMN regions (PCC and IPL) and with pericalcarine/cuneus, SPL, and ventral visual regions (cool colors). In attention > rest (warm colors), there was increased connectivity with bilateral TPJ, cingulate, and right anterior insula. Full results are reported in Supporting Information Table 4.

Five seed regions associated with the DAN were entered into similar differential connectivity analyses. These included bilateral intraparietal sulcus (IPS) [−26 −74 48], [26 −74 48], bilateral putative human frontal eye fields (hFEF) [−32 10 54], [32 10 54], and putative supplementary

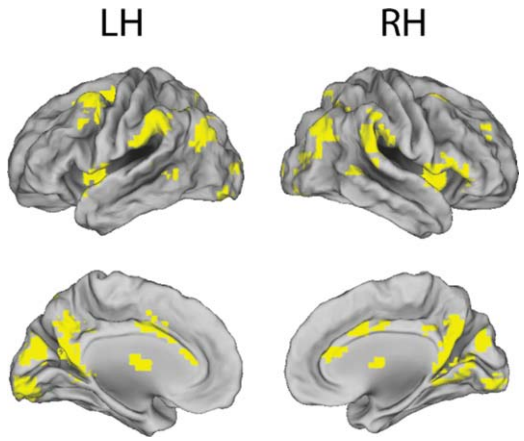

Figure 2.

Regions showing significant differences between rest and attention. Across models, regions showing significant differences between rest and attention networks were combined. This map of regions that shift between networks shows broad similarities to the community density map identified in Power et al. (2013; Figure 7) and uncertainty map in Lee et al. (2012; Figure 6). LH, left hemisphere; RH, right hemisphere. [Color figure can be viewed in the online issue, which is available at wileyonlinelibrary.com.]

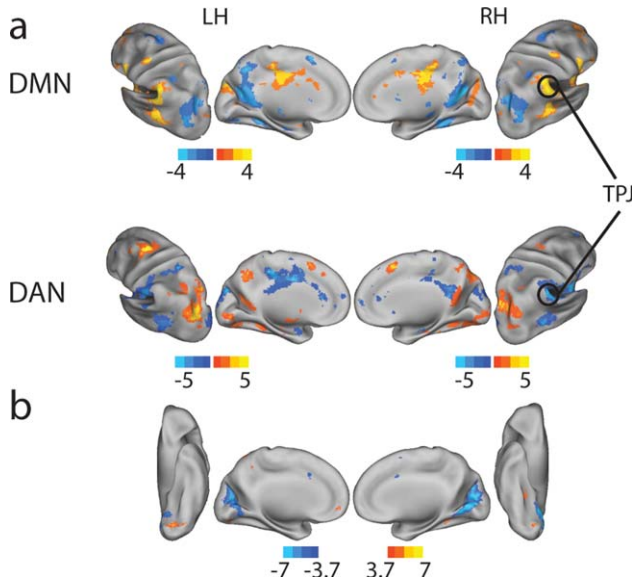

Figure 3.

Between-task differences in seed connectivity for core DMN, DAN, and visual regions. **a**) Consistency maps indicating consistent regions of significant difference in connectivity between rest and attention tasks, for seeds in the DMN and DAN. Top panel: Regions of significant ($P < 0.001$ uncorrected) difference between tasks for 1–4 DMN seeds (PCC, mPFC and bilateral IPL). Across 1–4 seeds rest showed greater connectivity with PCC and inferior parietal regions, while attention showed greater connectivity with cingulate, insula and TPJ. Bottom panel: Regions of significant ($P < 0.001$ uncorrected) difference between tasks for 1–5 DAN seeds (bilateral hFEF, bilateral IPS, SMA). Across 1–5 seeds attention showed stronger connectivity with IPS and hFEF, while rest showed greater connectivity with cingulate, occipitotemporal, SPL, and TPJ. **b**) Connectivity differences between tasks for core visual seed [2 −84 0], T-map shown at $P < 0.001$ uncorrected for display purposes. Warm colors = attention > rest, Cool colors = rest > attention. RH, right hemisphere, LH, left hemisphere; DMN, default mode network; DAN, dorsal attention network; TPJ, temporoparietal junction; PCC, posterior cingulate cortex; mPFC, medial prefrontal cortex; IPL, inferior parietal lobule; hFEF, putative human frontal eye fields; IPS, intraparietal sulcus; SMA, supplementary motor area; SPL, superior parietal lobule. [Color figure can be viewed in the online issue, which is available at wileyonlinelibrary.com.]

motor area (SMA) [2 26 48] (Supporting Information Fig. 4b). Consistency maps indicating regions of significant difference for rest > attention for 1–5 DAN seeds are shown in Figure 3a (lower panel). In rest > attention (cool colors) there was increased connectivity with bilateral TPJ, cingulate, and anterior insula and decreased connectivity near putative hFEF; in attention > rest (warm colors) the DAN seeds showed greater connectivity with DAN regions, including bilateral IPS and hFEF, as well as with visual regions. Full results in Supporting Information Table 4.

Finally, a seed region centered in the region of overlap for the visual networks across tasks ([2 −84 0]) was entered into a seed analysis (thresholded t-statistic maps shown in Fig. 3b). This region showed increased connectivity with a large cuneus cluster for rest > attention ([10 −58 −4], $n = 2{,}754$, $Z = 5.5$), as well as left superior temporal ([−48 10 −8], $n = 167$, $Z = 4.1$) and cerebellum ([−26 −50 −30], $n = 137$, $Z = 5.4$). For attention > rest there was increased connectivity to left lingual gyrus ([−16 −78 −12], $n = 182$, $Z = 4.4$).

Taken together these results show evidence for greater connectivity within the DMN at rest and within the DAN during attention. This analysis also underscored flexibility of regions such as the TPJ, SPL and insular cortex which were differently associated with both DAN and DMN seeds depending on the task. From a core region in the visual network there was both decreased connectivity with cuneus and increased connectivity with ventral lingual regions, consistent with both changes in the topography of this network during between tasks and modulation of connectivity within this network.

Connectivity Changes with Flexible Regions

Two regions identified as grouping with the DAN or DMN networks depending on the task, the left MFG and left TPJ, were entered into seed-based analyses, to compare connectivity patterns between tasks. These regions were chosen as examples of flexible regions for follow-up analyses as they showed consistent, and opposing, differences in network membership across the 6 and 7 cluster models (Table I; Supporting Information Table 2). The TPJ coordinate ([−60 −42 43]) was chosen in the region of overlap for DAN and DMN during rest and attention, respectively. The MFG coordinate ([−34 21 58]) was chosen in the region of overlap for DMN and DAN during attention and rest, respectively (Supporting Information Fig. 4c,d). Left panels of Figure 4 show average positive and negative connectivity patterns for the left TPJ [−60 −42 34] and MFG [−34 21 58]. For the left temporoparietal junction (LTPJ), difference maps in the right panels show enhanced connectivity with DMN regions such as PCC ([−4 −50 18], $n = 1{,}274$, $Z = 4.5$), mPFC ([2 62 6], $n = 2{,}692$, $Z = 5.1$), bilateral hippocampus ([−26 −18 −20], $n = 272$, $Z = 5.0$; [20 −16 −20], $n = 208$, $Z = 4.8$), anterior temporal ([−36 10 −14], $n = 133$, $Z = 4.6$; [−56 −6 −16], $n = 222$, $Z = 4.4$), bilateral inferior parietal ([52 −56 30], $n = 284$, $Z = 4.4$; [−44 −58 22], $n = 370$, $Z = 4.1$) and paracentral lobule ([−8 −20 64], $n = 215$, $Z = 4.3$) during attention > rest (cool colors) and enhanced connectivity with bilateral IPS ([32 −68 38], $n = 4{,}035$, $Z = 5.7$; [−24 −68 28], $n = 3{,}926$, $Z = 5.0$), DLPFC ([44 8 32], $n = 201$, $Z = 4.0$) and hFEF ([30 2 22], $n = 242$, $Z = 3.8$) during rest > attention (warm colors). For the left MFG (Fig. 4, second

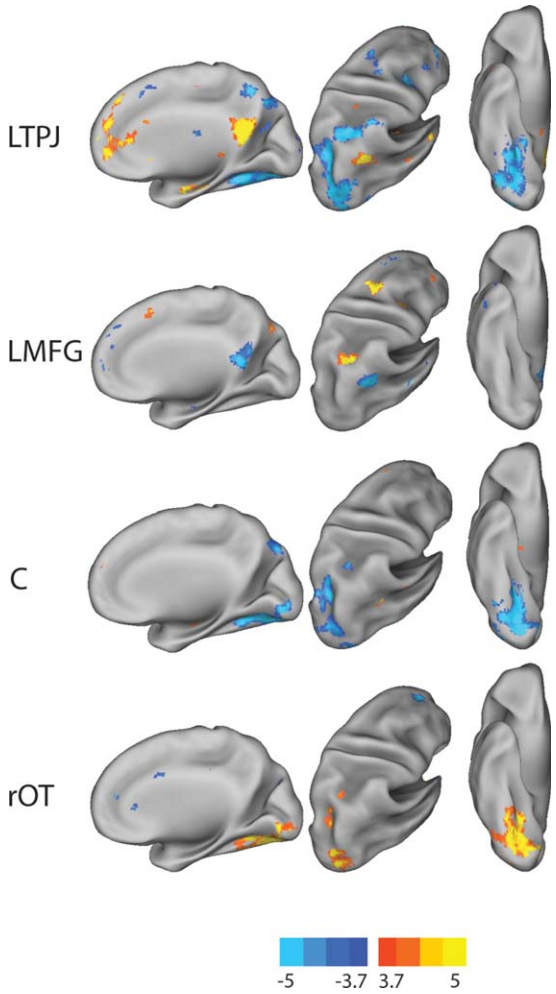

Figure 4.

Seed correlation maps for rest versus attention with flexible regions. Color maps indicate T-values. All shown at $P < 0.001$ uncorrected for display purposes. Right hemispheres are shown. Warm colors = attention > rest, cool colors = rest > attention. Top panel: LTPJ seed. DMN regions such as PCC and mPFC (in warm colors) showed greater connectivity during attention, while regions of the IPS and hFEF showed greater connectivity at rest (cool colors). Second panel from the top: LMFG seed. DMN regions such as PCC (in cool colors) showed greater connectivity during rest, while regions of the IPS and hFEF showed greater connectivity during attention (warm colors). Second panel from the bottom: Cuneus (C) seed showed stronger connectivity to ventral and dorsal visual regions at rest. Bottom panel: Right occipitotemporal (rOT) seed showed greater connectivity with dorsal and ventral visual regions during attention. Right hemispheres are shown. LTPJ, left temporoparietal junction; LMFG, left middle frontal gyrus; DMN, default mode network; PCC, posterior cingulate cortex, mPFC, medial prefrontal cortex; PC, pericalcaine; rOT, right occipitotemporal; hFEF, putative human frontal eye fields; IPS, intraparietal sulcus. [Color figure can be viewed in the online issue, which is available at wileyonlinelibrary.com.]

row from the top), this analysis showed increased connectivity with DMN regions such as posterior cingulate ([−10 −56 30], $n = 881$, $Z = 4.4$), bilateral IPL ([−48 −68 30], $n = 249$, $Z = 4.6$; [52 −52 26], $n = 353$, $Z = 4.3$), medial PFC ([−2 62 −6], $n = 1{,}086$, $Z = 4.3$) during rest > attention, and increased connectivity with DAN regions such as right MFG ([30 4 60], $n = 151$, $Z = 5.4$), and bilateral IPS ([30 −52 46], $n = 142$, $Z = 4.1$; [−36 −50 46], $n = 226$, $Z = 3.74$) for attention > rest.

We also looked at regions with differential membership to the visual network depending on the task (Fig. 4, rows 3 and 4). These seeds were chosen as the cuneus and right occipitotemporal peaks of the clusters that varied in membership to the visual network between tasks (Table I). The cuneus seed (Table I; [−6 −76 22]) showed greater connectivity with bilateral dorsal (posterior IPS: [−14 −76 40], $n = 652$, $Z = 4.8$; [32 −66 34], $n = 975$, $Z = 4.2$) and ventral (fusiform: [28 −66 6], $n = 2{,}557$, $Z = 4.9$) visual regions at rest. This region showed greater connectivity with bilateral occipitotemporal cortex ([42 −50 12], $n = 276$, $Z = 4.6$; [−60 −56 10], $n = 147$, $Z = 4.2$), and right hippocampus ([18 −12 −18], $n = 119$, $Z = 4.2$) during attention (> rest). The right occipitotemporal seed (Table I; [50 −72 18]) showed the opposite pattern, that is greater connectivity with bilateral dorsal ([−24 −70 48], $n = 127$, $Z = 3.9$; [26 −54 36], $n = 183$, $Z = 3.8$) and ventral ([−14 −79 −4], $n = 5{,}080$, $Z = 5.4$) visual regions, and posterior left inferior frontal gyrus (IFG) ([−44 4 38], $n = 386$, $Z = 4.6$) during attention > rest. This region showed greater connectivity with right MFG ([26 48 20], $n = 153$, $Z = 4.6$) and left occipitotemporal ([−58 −62 10], $n = 211$, $Z = 4.3$) regions during rest > attention.

Temporal Nonstationarity of Flexible Regions

Our analyses identified several regions that showed variable connectivity with DMN, DAN, and visual networks depending on the task state. We investigated the temporal nonstationarity of network connectivity to determine whether during rest these flexible regions showed momentary connectivity with DMN and DAN networks, which may presage the observed flexibility in connectivity between task states.

Figure 5 shows the results from temporal clustering of volumes associated with LTPJ peaks during rest and attention (top and bottom rows), in relation to seed connectivity maps (middle row). At rest, two temporal patterns were seen across all subjects, 48 and 52% of the time, respectively. One spatial pattern was strongly correlated to resting seed connectivity (0.6) and weakly correlated to attention seed connectivity (0.08), while the other was similarly correlated to both (0.43 and 0.48). Notably, the attention seed connectivity map includes bright colors near the PCC and medial PFC regions typically associated with the DMN; these regions were also included in the rightmost temporal cluster. During attention this pattern was shifted. One cluster was predominantly correlated to the attention

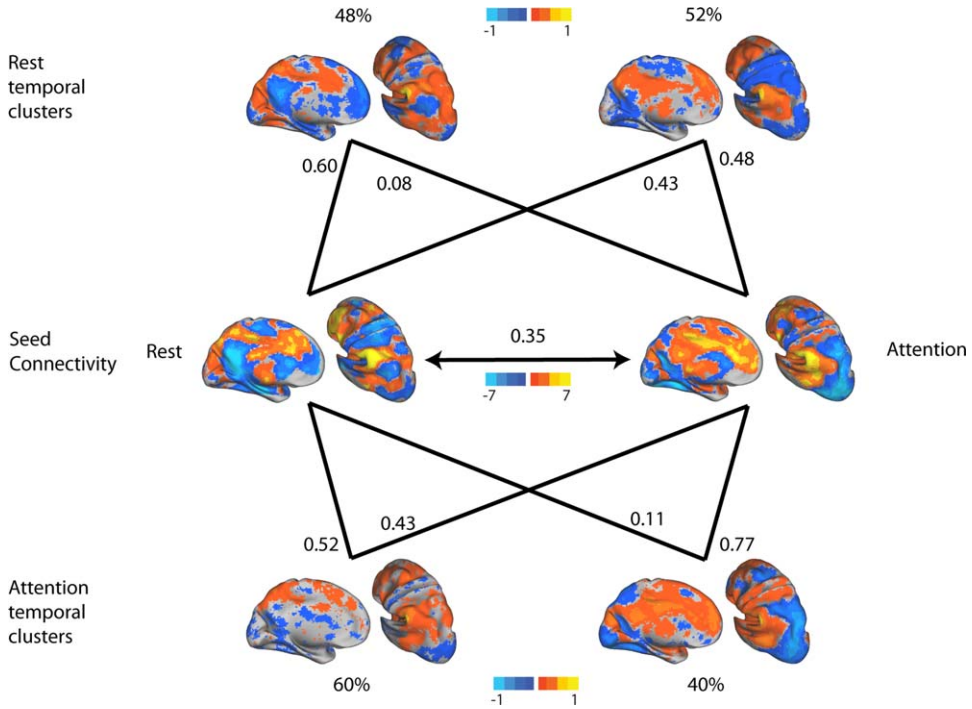

Figure 5.

Temporal nonstationarity of LTPJ connectivity. The middle row shows unthresholded T-statistic maps for group-level connectivity results from the LTPJ seed during rest and attention tasks. The spatial correlation between the rest and attention seed maps is 0.35. The top row shows the two temporal clusters during the resting task and the bottom row shows the two temporal clusters during the attention task. Links between temporal clusters and seed connectivity maps indicate the spatial correlation between them. This figure shows that at rest, one temporal cluster is predominantly correlated to the resting seed map, while the other shows a strong correlation to both attention and rest seed maps. The converse is apparent in the bottom row for the temporal clusters during attention. Note that the attention seed map includes PCC and medial PFC regions typically associated with the DMN. These regions are included in the top right resting temporal cluster, but not the leftmost. Top and bottom row color maps indicate standardized deviation from the mean. Left hemispheres are shown. LTPJ, left temporoparietal junction; PCC, posterior cingulate cortex; mPFC, medial prefrontal cortex. [Color figure can be viewed in the online issue, which is available at wileyonlinelibrary.com.]

seed map (0.77 vs. 0.11), while the other was more balanced (0.52 and 0.43). Thus, consistent with the overall shift in connectivity observed in the clustering and seed-based analyses, TPJ modes during attention showed increased involvement of core DMN regions, relative to rest. A follow-up analysis merged both tasks into a single clustering analysis. This showed that at rest 42% of volumes grouped with the DMN cluster and 57% grouped with the DAN cluster. During attention there was a shift in temporal allocation: 65% grouped with the DMN cluster and 35% with the DAN cluster.

Figure 6 shows the results for temporal clustering of volumes associated with LMFG peaks during rest and attention (top and bottom rows). Similar to the LTPJ seed at rest, one temporal cluster showed relatively stronger spatial correlation with the resting seed connectivity map, while the other showed stronger spatial correlation with the attention seed connectivity map. During attention, the temporal cluster that more closely resembled the attention seed map was more frequent (65% of the temporal volumes). Note that at rest one temporal cluster (on the left) includes PCC, mPFC and IPL regions typically associated with the DMN, while the other cluster covers intraparietal and dorsal frontal regions more commonly associated with the DAN. A follow-up analysis merged both tasks into one clustering analysis. At rest 50% of volumes grouped with the DMN cluster and 50% grouped with the DAN cluster, while during attention 25% grouped with the DMN cluster, and 75% with the DAN cluster.

We additionally examined temporal nonstationarity of two visual regions that showed differential membership to the visual network depending on the task. Figure 7 shows the results of temporal clustering of peak volumes for the cuneus seed. The top row shows temporal clusters identified at rest and demonstrates that there is variability in the recruitment of dorsal and ventral visual regions. As with

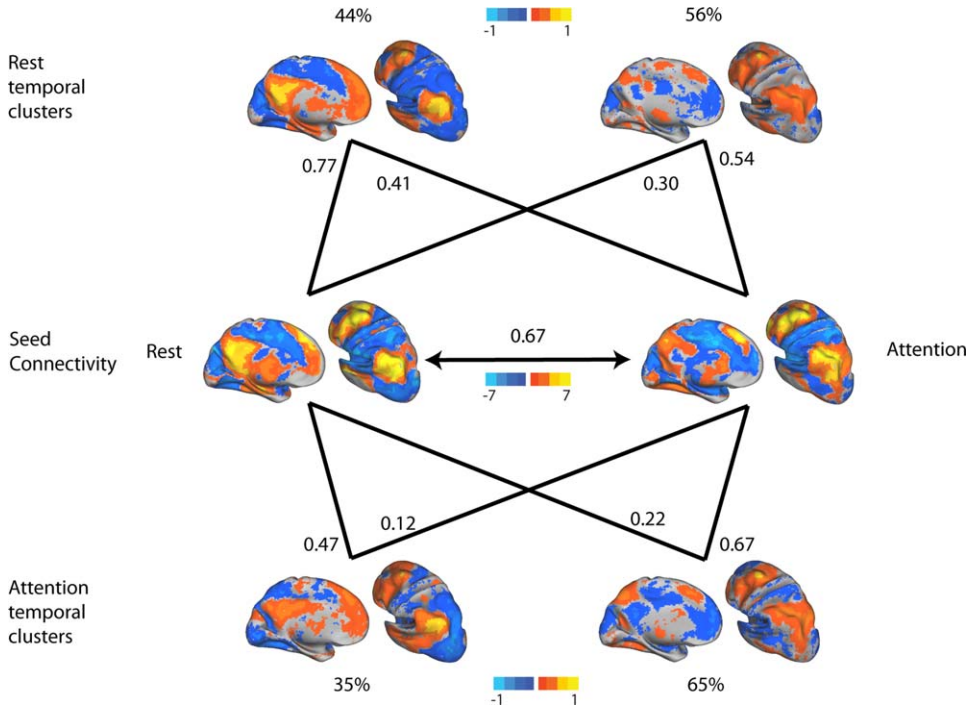

Figure 6.

Temporal nonstationarity of LMFG connectivity. The middle row shows unthresholded T-statistic maps for group-level connectivity results from the LMFG seed during rest and attention tasks. The spatial correlation between the rest and attention seed maps is 0.67. The top row shows the two temporal clusters during the resting task and the bottom row shows the two temporal clusters during the attention task. Links between temporal clusters and seed connectivity maps indicate the spatial correlation between them. Note that the rest seed map includes PCC and medial PFC regions typically associated with the DMN. These regions are included in the top left resting temporal cluster, but not the rightmost cluster. Top and bottom row color maps indicate standardized deviation from the mean. Left hemispheres are shown. LMFG, left middle frontal gyrus; DMN, default mode network; PCC, posterior cingulate cortex; PFC, prefrontal cortex. [Color figure can be viewed in the online issue, which is available at wileyonlinelibrary.com.]

the LMFG and LTPJ seeds, similarity of temporal clusters to the attention seed map increased in the attention task; however, even at rest one of the temporal clusters showed greater correlation to the attention relative to resting map. Supporting Information Figure 6 shows similar results for the right occipitotemporal seed.

Results of the nonstationarity analyses demonstrate that even at rest flexible regions show momentary connectivity patterns that recruited, in the case of LTPJ and LMFG, core regions of both the DMN and DAN. This suggests that condition-dependent changes in connectivity may be best understood as shifts in the amount of time specific connections are engaged rather than a full switch in connectivity between networks.

DISCUSSION

In this study, we aimed to better understand whether the topography of functional networks changes between resting and attentive states, compared to the alternative in which network structure is preserved, but connectivity is modulated within and between networks. We used a data driven approach to identify a similar set of networks in both attention and rest, and compared the spatial extent of these networks. This analysis showed that while similar networks could be identified, a set of flexible regions near internetwork borders showed stronger connectivity with different networks depending on the task state. Follow-up seed-based analyses from both core and flexible regions found evidence for within-network connectivity modulation, and provided converging evidence for the flexibility of regions such as the posterior MFG and TPJ. Finally, we investigated how connectivity patterns of flexible regions changed across time within tasks, and found that variability in the spatial connectivity patterns for flexible regions at rest were suggestive of the changes observed between conditions.

Interestingly, the regions identified as flexible in our study largely concur with several recent investigations into

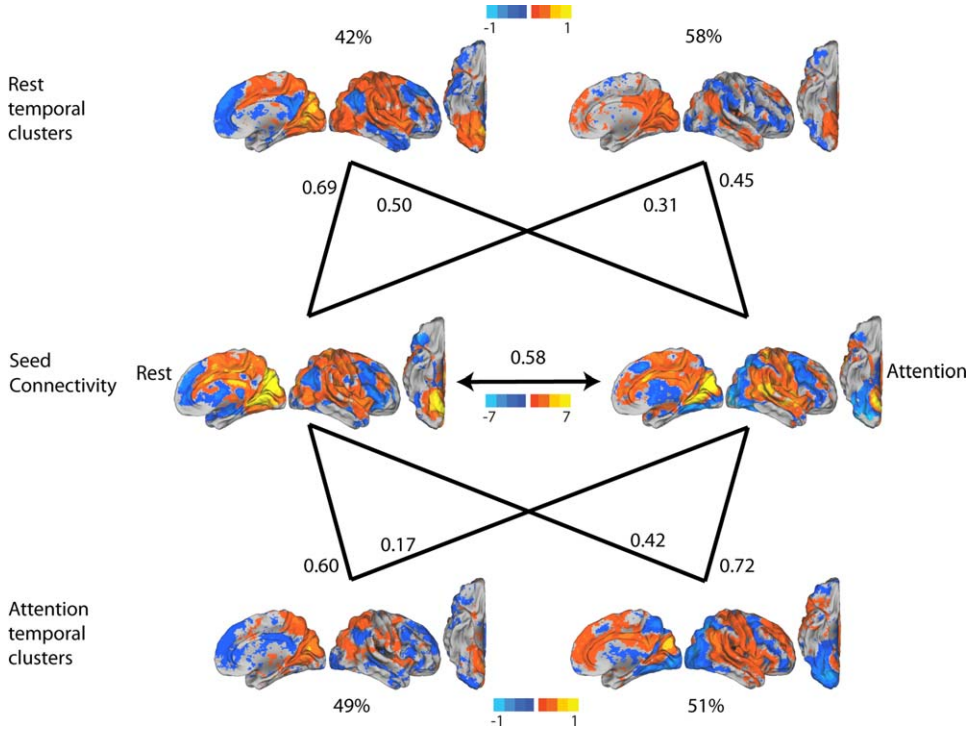

Figure 7.

Temporal nonstationarity of cuneus seed connectivity. The middle row shows unthresholded T-statistic maps for group-level connectivity results from the cuneus seed during rest and attention tasks. The spatial correlation between the rest and attention seed maps is 0.58. The top row shows the two temporal clusters during the resting task and the bottom row shows the two temporal clusters during the attention task. Links between temporal clusters and seed connectivity maps indicate the spatial correlation between them. Note that at rest there is greater recruitment of dorsal and ventral visual regions, relative to attention, consistent with differences shown in Figure 3. This between-task difference is reflected in the two temporal clusters seen at rest, the leftmost of which shows more extensive dorsal and ventral visual regions. Top and bottom row color maps indicate standardized deviation from the mean. Left hemispheres are shown. [Color figure can be viewed in the online issue, which is available at wileyonlinelibrary.com.]

regions showing "hub"-like properties. Power et al. [2013] combined graph theoretical with voxel-wise analyses to identify a set of candidate hubs, defined as regions with the potential to connect multiple networks, rather than a perhaps more traditional definition of regions that show high connectivity density [Tomasi and Volkow, 2011]. These included anterior insula, dorsal medial PFC, dorsal PFC, lateral occipital-temporal and superior parietal regions. Lee et al. [2012] applied an uncertainty metric to their cluster-based parcellation of RSNs, to identify regions of maximal uncertainty. These authors found that greater uncertainty occurred in the language, frontoparietal and ventral-attention networks. It is notable that this uncertainty map bears resemblance in several regions to the candidate hubs in Power et al. [2013] and the regions of significant difference between attention and rest conditions identified here. The findings presented here complement this work by demonstrating that functional connectivity patterns of regions near internetwork borders may change depending on cognitive state.

Although resting-state functional connectivity is typically assessed using ICA or temporal correlations across the duration of a scan, several recent studies have highlighted the temporal variability of fMRI connectivity profiles [Kiviniemi et al., 2011; Rack-Gomer and Liu, 2012; Chang and Glover, 2010; Liu and Duyn, 2013; Allen et al., 2014]. This work builds on studies using techniques such as MEG, with inherently higher temporal resolution, which have shown evidence for nonstationarity in coherence patterns [de Pasquale et al., 2010; Hutchison et al., 2013; Larson-Prior et al., 2013] and interactions between multiple networks at rest [Marzetti et al., 2013]. In particular, Liu and Duyn [2013] used a modification of the point process approach to demonstrate that core DMN and DAN regions show activation peaks that covary with different sets of regions at different time points. This work

motivated us to look at variability in resting temporal connectivity in the flexible regions we identified. Specifically, we found that flexible regions show momentary associations with regions of both DMN and DAN regions at different time points during the resting scan. These findings suggest that spatial changes in functional connectivity from rest to attention may be understood as shifts into modes present but less prominent at rest, rather than a switch in network membership per se. It would be interesting to test this hypothesis looking at other regions that have been suggested to 'bridge' functional networks. For example, de Pasquale et al. [2013] identified functional cores in the PCC and SMA, defined as regions with the most statistically significant connections to other parts of the brain. These regions were integrated with default mode and somatomotor networks, respectively. Although largely segregated, connectivity of these two regions converged on medial components of the DMN, potentially allowing for internetwork interactions.

A number of studies have investigated differences between functional connectivity during rest and task states, with somewhat divergent findings. Converging evidence suggests that while there is a consistent network architecture across task and rest [Cole et al. 2014], small but important connectivity differences distinguish task conditions. In the context of continuous visual attention, density of functional connections has been shown to decrease during attention relative to rest, particularly in regions weakly engaged by the task [Tomasi et al., 2013]. Golland et al. [2008] showed that relatively similar intrinsic and extrinsic networks could be identified during passive viewing. A recent combined fMRI and MEG study suggested that connectivity differences between rest and free viewing occur mainly as within- and between-network modulations in connectivity, with relatively preserved network structure [Betti et al., 2013]. Several studies have also explored connectivity differences across sets of tasks. Mennes et al. [2013] described differences between functional connectivity profiles during rest and a set of event-related tasks. They found that patterns of intrinsic and task-driven functional connectivity showed voxel-wise differences, particularly for sensory, motor and subcortical regions. Volumetric expansion of motor and visual networks has also been shown during an auditory oddball task, relative to rest [Arbabshirani et al., 2013]. These findings are somewhat at odds with a recent study showing that among 10 brain networks, the frontoparietal network shows the greatest variability in connectivity with other nodes in the brain [Cole et al., 2013], across a number of task states, suggesting that regions of this network are the most "hub"-like. In a separate study, it has also been shown that during a recollection paradigm, the DMN reconfigured into core and transitional subsystems, the latter of which enhanced integration with frontoparietal regions [Fornito et al., 2012]. The results reported here using whole-brain voxel-wise comparisons of network membership could be interpreted as reconciling these various accounts, showing that across task states there may be dynamic shifts in network membership across multiple networks, particularly at internetwork border regions, as predicted by a community density model of network hubs [Power et al., 2013]. Notably, this finding may be more evident using a voxel-wise analysis approach as opposed to a priori definition of ROIs.

A recent approach to comparing rest and task based connectivity is meta-analytic connectivity modeling (MACM), reviewed in [Laird et al., 2013]. This approach uses databases such as BrainMap (http://brainmap.org; [Fox and Lancaster, 2002; Laird et al., 2005]), which gather results from a large number of studies, to investigate patterns of task-based coactivations. While only a small number of studies to date have used MACM in conjunction with resting-state analyses (e.g., [Cieslik et al., 2013; Eickhoff et al., 2011; Jakobs et al., 2012]), both similarities and differences have been noted in the connectivity profiles obtained from these two methods. Laird et al. [2013] use V5 as an example to compare the coactivation map from the BrainMap database with a seed-based analysis of resting data. While a conjunction analysis identified a parieto-occipital network common to these approaches, the RSN analysis identified a more extensive connectivity network. The findings reported here generally agree with this work, showing that while there are broad similarities between resting and task-evoked networks, there are also some key differences.

One of the regions consistently showing connectivity differences across both the clustering and seed-based analyses was a portion of the TPJ. The TPJ is a functionally heterogeneous region that has been previously been implicated in attentional orienting [Cieslik et al., 2011], theory of mind [Young et al., 2010] and sensory integration [Jakobs et al., 2012]. To better understand this apparent heterogeneity, clustering of structural connectivity information has been used to divide the TPJ into three subregions, which functionally connected to regions of the default mode, salience, and frontoparietal networks, respectively [Rushworth et al., 2006]. Seed and temporal nonstationarity analyses showed that this region made connections with regions of the DAN and DMN that differed both between tasks and across the RSN. Spatial clustering also showed this region was near the intersection of these three networks. Our work provides some additional insight into the function of the TPJ as a region at the interface between multiple networks that may explain its role in a wide range of cognitive tasks.

In addition to connectivity differences in the DMN and DAN, we also observed prominent differences in the spatial extent of the visual network. Moving from 6 to 7 spatial clusters, segregation of the visual network was more prominent in the attention task. This is in agreement with previous work showing widespread connectivity within

visual occipital regions at rest that becomes more specific during vision tasks [Nir et al., 2006]. Evidence for task-specific shifts in visual connectivity, for example between visual and language regions during movie viewing with social content, has also been reported [Betti et al., 2013]. Our analysis showed that some regions (cuneus) decoupled from dorsal and ventral visual regions during attention, while others (right occipitotemporal) showed greater connectivity with these regions. Nonstationarity analysis using these seeds suggested that, similar to TPJ and MFG, even at rest there was variability in moment-to-moment connectivity that mirrored connectivity patterns at rest and attention. Together these findings suggest that in situations when individuals are attending to changing visual input, both the amplification of connections within ICNs and reconfiguration of peripheral connectivity occurs.

The task used here required participants to learn the arrangement of four visually salient landmarks as they were passively guided through a virtual city. This is somewhat different from previous studies addressing a similar question which have used passive viewing of scenes [Golland et al., 2008; Betti et al., 2013] or visual target tracking [Tomasi et al., 2013]. Spatial learning is known to engage a widespread network of regions including the hippocampus and parahippocampal cortex, precuneus, posterior and inferior parietal, and prefrontal regions [Burgess et al., 2001; Byrne et al., 2007; Hartley et al., 2003; Iaria et al., 2003; Maguire et al., 1998]. While this is not a 'pure' spatial attention task and also relies on working memory, object recognition and memory encoding, sustained attention to a changing visual display was consistently engaged across the duration of the scan. As the goal of this study was to compare networks engaged during an attentionally demanding task against resting networks, there is no control condition, and it is difficult to say which connectivity changes from rest are due specifically to attention relative to working memory or spatial learning. However, as connectivity values were obtained by averaging over 5 min, continuous attention to a changing visual display is the most consistent cognitive process and this task has the advantage of not requiring target detection decisions, motor responses or social/language content.

Several recent studies have applied clustering approaches to divide the brain or specific subregions into sets of voxels that show similar time-courses or connectivity patterns. A noted challenge in both this approach and ICA is determining the optimal number of clusters or components [Kelly et al., 2010; Shen et al., 2013]. Several authors have also observed hierarchical subdivisions [Wang and Li, 2013; Lee et al., 2012] suggesting there may not be one but many optimal solutions at different levels of resolution. Indeed, cluster numbers on the order of hundreds essentially identify localized ROIs rather than distributed networks [Shen et al., 2013]. Here we applied both a heuristic metric (the ability to match clusters across conditions) and a silhouette metric [Kaufman and Rousseeuw, 1990] approach to determine an appropriate number of spatial clusters. While the heuristic approach may have enforced greater similarity between the networks derived from different tasks, both the regions of significant difference and the way in which networks preferentially split for larger cluster numbers were informative for understanding functional connectivity differences between these tasks.

A number of data-driven approaches have been applied to identify distributed networks or ROIs from time-course or connectivity data, including ICA [Smith et al., 2009], spectral clustering [Shen et al., 2013], k-means and fuzzy clustering [Kahnt et al., 2012; Lee et al., 2012], and normalized-cut algorithms [Shen et al., 2010]. At the whole-brain network level these have provided largely complementary results. Clustering approaches have an advantage over ICA insofar as that they do not require manual selection of components: every voxel is assigned to a particular cluster. However, conversely, the ability of ICA to identify and remove spatiotemporal noise patterns is helpful. A recent study directly compared hierarchical clusters to ICA-derived components and noted both similarities and differences [Wang and Li, 2013]. While 8 of the derived networks showed spatial overlap, the authors note that ICA frequently identifies lateralized frontoparietal components [Smith et al., 2009], while clustering approaches are less likely to do so due to the overlapping voxels that would be part of both the left- and right-lateralized networks. Interestingly, meta-analytic task coactivation studies tend to identify bilateral dorsal attention or frontoparietal networks [Toro et al., 2008].

There are several limitations associated with this study. A longer resting scan could have enabled more reliable identification of networks, however, in clinical studies, particularly those involving children, resting scans on the order of 5–7 min are not uncommon (e.g., [Di Martino et al., 2013]). Finally, a small number of participants were included in the analyses described here, relative to many RSN (e.g., [Tomasi and Volkow, 2012] and MACM studies which pool data across hundreds of subjects and multiple tasks [Toro et al., 2008].

CONCLUSION

In conclusion, we present here an investigation into spatial and temporal connectivity differences in functional networks identified at rest and during a state of continuous visual attention to a changing visual display. Our results suggest that in addition to within-network connectivity modulation, and consistent with a model of functional hubs at regions of high community density, border regions between networks including the DAN, DMN, and visual network, are flexible across task states. Moreover, we show that this flexibility may be predicted from moment-to-moment variability in resting connectivity patterns in these regions. Data-driven connectivity clustering has previously been applied to identify regions of differential functional connectivity in clinical conditions [Bray et al., 2013].

Variability in the flexibility of internetwork borders between rest and task may provide an additional tool for investigating the basis of cognitive difficulties in individuals with brain disorders. Indeed, the ability for specific regions to dynamically link ICNs under different task conditions may play an important role in behavioral flexibility.

ACKNOWLEDGMENTS

The authors would like to thank the Seaman Family MR Centre, the Hotchkiss Brain Institute, and Sarah Vinette.

REFERENCES

Al-Aidroos N, Said CP, Turk-Browne NB (2012): Top-down attention switches coupling between low-level and high-level areas of human visual cortex. Proc Natl Acad Sci USA 109:14675–14680.

Allen EA, Damaraju E, Plis SM, Erhardt EB, Eichele T, Calhoun VD (2014): Tracking whole-brain connectivity dynamics in the resting state. Cereb Cortex 24:663–676.

Arbabshirani MR, Havlicek M, Kiehl KA, Pearlson GD, Calhoun VD (2013): Functional network connectivity during rest and task conditions: A comparative study. Hum Brain Mapp 34: 2959–2971.

Arnold AE, Protzner AB, Bray S, Levy RM, Iaria G (2014): Neural network configuration and efficiency underlies individual differences in spatial orientation ability. J Cogn Neurosci 26:380–394.

Betti V, Della Penna S, de Pasquale F, Mantini D, Marzetti L, Romani GL, Corbetta M (2013): Natural scenes viewing alters the dynamics of functional connectivity in the human brain. Neuron 79:782–797.

Bezdec JC (1981): Pattern Recognition with Fuzzy Objective Function Algorithms. New York: Plenum Press.

Biswal B, Yetkin FZ, Haughton VM, Hyde JS (1995): Functional connectivity in the motor cortex of resting human brain using echo-planar MRI. Magn Reson Med 34:537–541.

Bray S, Hoeft F, Hong DS, Reiss AL (2013): Aberrant functional network recruitment of posterior parietal cortex in turner syndrome. Hum Brain Mapp 34:3117–128.

Brookes MJ, Woolrich M, Luckhoo H, Price D, Hale JR, Stephenson MC, Barnes GR, Smith SM, Morris PG (2011): Investigating the electrophysiological basis of resting state networks using magnetoencephalography. Proc Natl Acad Sci USA 108:16783–16788.

Buckner RL, Sepulcre J, Talukdar T, Krienen FM, Liu H, Hedden T, Andrews-Hanna JR, Sperling RA, Johnson KA (2009): Cortical hubs revealed by intrinsic functional connectivity: Mapping, assessment of stability, and relation to Alzheimer's disease. J Neurosci 29:1860–1873.

Burgess N, Maguire EA, Spiers HJ, O'Keefe J (2001): A temporoparietal and prefrontal network for retrieving the spatial context of lifelike events. Neuroimage 14:439–453.

Byrne P, Becker S, Burgess N (2007): Remembering the past and imagining the future: A neural model of spatial memory and imagery. Psychol Rev 114:340–375.

Chang C, Glover GH (2010): Time-frequency dynamics of resting-state brain connectivity measured with fMRI. Neuroimage 50: 81–98.

Cieslik EC, Zilles K, Grefkes C, Eickhoff SB (2011): Dynamic interactions in the fronto-parietal network during a manual stimulus-response compatibility task. Neuroimage 58:860–869.

Cieslik EC, Zilles K, Caspers S, Roski C, Kellermann TS, Jakobs O, Langner R, Laird AR, Fox PT, Eickhoff SB (2013): Is There "One" DLPFC in cognitive action control? evidence for heterogeneity from co-activation-based parcellation. Cereb Cortex 23: 2677–2689.

Cole MW, Pathak S, Schneider W (2010): Identifying the brain's most globally connected regions. Neuroimage 49:3132–3148.

Cole MW, Reynolds JR, Power JD, Repovs G, Anticevic A, Braver TS (2013): Multi-task connectivity reveals flexible hubs for adaptive task control. Nat Neurosci 16:1348–1355.

Cole MW, Bassett DS, Power JD, Braver TS, Petersen SE (2014): Intrinsic and task-evoked network architectures of the human brain. Neuron 83:238–251.

Dagli MS, Ingeholm JE, Haxby JV (1999): Localization of cardiac-induced signal change in fMRI. Neuroimage 9:407–415.

Damoiseaux JS, Rombouts SA, Barkhof F, Scheltens P, Stam CJ, Smith SM, Beckmann CF (2006): Consistent resting-state networks across healthy subjects. Proc Natl Acad Sci USA 103: 13848–13853.

de Pasquale F, Della Penna S, Snyder AZ, Lewis C, Mantini D, Marzetti L, Belardinelli P, Ciancetta L, Pizzella V, Romani GL, et al. (2010): Temporal dynamics of spontaneous MEG activity in brain networks. Proc Natl Acad Sci USA 107:6040–6045.

de Pasquale F, Della Penna S, Snyder AZ, Marzetti L, Pizzella V, Romani GL, Corbetta M (2012): A cortical core for dynamic integration of functional networks in the resting human brain. Neuron 74:753–764.

de Pasquale F, Sabatini U, Della Penna S, Sestieri C, Caravasso CF, Formisano R, Péran, P. (2013): The connectivity of functional cores reveals different degrees of segregation and integration in the brain at rest. Neuroimage 69:51–61.

Di Martino A, Zuo XN, Kelly C, Grzadzinski R, Mennes M, Schvarcz A, Rodman J, Lord C, Castellanos FX, Milham MP (2013): Shared and distinct intrinsic functional network centrality in autism and attention-deficit/hyperactivity disorder. Biol Psychiatry 74:623–632.

Eickhoff SB, Bzdok D, Laird AR, Roski C, Caspers S, Zilles K, Fox PT. (2011): Co-activation patterns distinguish cortical modules, their connectivity and functional differentiation. Neuroimage 57:938–949.

Fornito A, Harrison BJ, Zalesky A, Simons JS (2012): Competitive and cooperative dynamics of large-scale brain functional networks supporting recollection. Proc Natl Acad Sci USA 109: 12788–12793.

Fox MD, Snyder AZ, Vincent JL, Corbetta M, Van Essen DC, Raichle ME (2005): The human brain is intrinsically organized into dynamic, anticorrelated functional networks. Proc Natl Acad Sci USA 102:9673–9678.

Fox MD, Corbetta M, Snyder AZ, Vincent JL, Raichle ME. (2006): Spontaneous neuronal activity distinguishes human dorsal and ventral attention systems. Proc Natl Acad Sci 103:10046–10051.

Fox PT, Lancaster JL (2002): Opinion: Mapping context and content: the BrainMap model Nat Rev Neurosci 3:319–321.

Golland Y, Golland P, Bentin S, Malach R (2008): Data-driven clustering reveals a fundamental subdivision of the human cortex into two global systems. Neuropsychologia 46:540–553.

Greenberg AS, Verstynen T, Chiu YC, Yantis S, Schneider W, Behrmann M (2012): Visuotopic cortical connectivity

underlying attention revealed with white-matter tractography. J Neurosci 32:2773–2782.

Greicius MD, Supekar K, Menon V, Dougherty RF (2009): Resting-state functional connectivity reflects structural connectivity in the default mode network. Cereb Cortex 19:72–78.

Hartley T, Maguire EA, Spiers HJ, Burgess N (2003): The well-worn route and the path less traveled: Distinct neural bases of route following and wayfinding in humans. Neuron 37:877–888.

He BJ, Snyder AZ, Zempel JM, Smyth MD, Raichle ME (2008): Electrophysiological correlates of the brain's intrinsic large-scale functional architecture. Proc Natl Acad Sci USA 105: 16039–16044.

Hipp JF, Hawellek DJ, Corbetta M, Siegel M, Engel AK (2012): Large-scale cortical correlation structure of spontaneous oscillatory activity. Nat Neurosci 15:884–890.

Honey CJ, Sporns O, Cammoun L, Gigandet X, Thiran JP, Meuli R, Hagmann P (2009): Predicting human resting-state functional connectivity from structural connectivity. Proc Natl Acad Sci USA 106:2035–2040.

Hutchison RM, Womelsdorf T, Allen EA, Bandettini PA, Calhoun VD, Corbetta M, Della Penna S, Duyn JH, Glover GH, Gonzalez-Castillo J, Handwerker DA, Keilholz S, Kiviniemi V, Leopold DA, de Pasquale F, Sporns O, Walter M, Chang C. (2013): Dynamic functional connectivity: Promise, issues, and interpretations. Neuroimage 80:360–378.

Iaria G, Petrides M, Dagher A, Pike B, Bohbot VD (2003): Cognitive strategies dependent on the hippocampus and caudate nucleus in human navigation: Variability and change with practice. J Neurosci 23:5945–5952.

Jakobs O, Langner R, Caspers S, Roski C, Cieslik EC, Zilles K, Laird AR, Fox PT, Eickhoff SB (2012): Across-study and within-subject functional connectivity of a right temporo-parietal junction subregion involved in stimulus-context integration. Neuroimage 60:2389–2398.

Kahnt T, Chang LJ, Park SQ, Heinzle J, Haynes JD (2012): Connectivity-based parcellation of the human orbitofrontal cortex. J Neurosci 32:6240–6250.

Kaufman L, Rousseeuw PJ (1990): Finding Groups in Data: An Introduction to Cluster Analysis. Hoboken, NJ: Wiley.

Kelly C, Uddin LQ, Shehzad Z, Margulies DS, Castellanos FX, Milham MP, Petrides M (2010): Broca's region: Linking human brain functional connectivity data and non-human primate tracing anatomy studies. Eur J Neurosci 32:383–398.

Kiviniemi V, Vire T, Remes J, Elseoud AA, Starck T, Tervonen O, Nikkinen J (2011): A sliding time-window ICA reveals spatial variability of the default mode network in time. Brain Connect 1:339–347.

Laird AR, Lancaster JL, Fox PT (2005): BrainMap: The social evolution of a human brain mapping database. Neuroinformatics 3:65–78.

Laird AR, Eickhoff SB, Rottschy C, Bzdok D, Ray KL, Fox PT (2013): Networks of task co-activations. Neuroimage 80:505–514.

Larson-Prior LJ, Oostenveld R, Della Penna S, Michalareas G, Prior F, Babajani-Feremi A, Schoffelen JM, Marzetti L, de Pasquale F, Di Pompeo F, Stout J, Woolrich M, Luo Q, Bucholz R, Fries P, Pizzella V, Romani GL, Corbetta M, Snyder AZ, WU-Minn HCP Consortium. (2013): Adding dynamics to the Human Connectome Project with MEG. Neuroimage 80:190–201.

Lee MH, Hacker CD, Snyder AZ, Corbetta M, Zhang D, Leuthardt EC, Shimony JS (2012): Clustering of resting state networks. PLoS One 7:e40370.

Liu X, Duyn JH (2013): Time-varying functional network information extracted from brief instances of spontaneous brain activity. Proc Natl Acad Sci USA 110:4392–4397.

Liu X, Zhu XH, Qiu P, Chen W (2012): A correlation-matrix-based hierarchical clustering method for functional connectivity analysis. J Neurosci Methods 211:94–102.

Maguire EA, Burgess N, Donnett JG, Frackowiak RS, Frith CD, O'Keefe J (1998): Knowing where and getting there: A human navigation network. Science 280:921–924.

Marzetti L, Della Penna S, Snyder AZ, Pizzella V, Nolte G, de Pasquale F, Romani GL, Corbetta M (2013): Frequency specific interactions of MEG resting state activity within and across brain networks as revealed by the multivariate interaction measure. Neuroimage 79:172–183.

Mazaika P, Hoeft F, Glover G, Reiss A (2009): Methods and Software for fMRI Analysis for Clinical Subjects. In: Human Brain Mapping Conference, San Francisco, CA, USA.

Mennes M, Kelly C, Colcombe S, Castellanos FX, Milham MP (2013): The extrinsic and intrinsic functional architectures of the human brain are not equivalent. Cereb Cortex 23:223–229.

Murphy K, Birn RM, Handwerker DA, Jones TB, Bandettini PA (2009): The impact of global signal regression on resting state correlations: Are anti-correlated networks introduced? Neuroimage 44:893–905.

Niazy RK, Xie J, Miller K, Beckmann CF, Smith SM (2011): Spectral characteristics of resting state networks. Prog Brain Res 193:259–276.

Nichols TE, Holmes AP (2002): Nonparametric permutation tests for functional neuroimaging: A primer with examples. Hum Brain Mapp 15:1–25.

Nir Y, Hasson U, Levy I, Yeshurun Y, Malach R (2006): Widespread functional connectivity and fMRI fluctuations in human visual cortex in the absence of visual stimulation. Neuroimage 30:1313–1324.

Nir Y, Mukamel R, Dinstein I, Privman E, Harel M, Fisch L, Gelbard-Sagiv H, Kipervasser S, Andelman F, Neufeld MY, Kramer U, Arieli A, Fried I, Malach R. (2008): Interhemispheric correlations of slow spontaneous neuronal fluctuations revealed in human sensory cortex. Nat Neurosci 11:1100–1108.

Power JD, Cohen AL, Nelson SM, Wig GS, Barnes, KA, Church JA, Vogel AC, Laumann TO, Miezin FM, Schlaggar BL, Petersen SE. (2011): Functional network organization of the human brain. Neuron 72:665–678.

Power JD, Barnes KA, Snyder AZ, Schlaggar BL, Petersen SE (2012): Spurious but systematic correlations in functional connectivity MRI networks arise from subject motion. Neuroimage 59:2142–2154.

Power JD, Schlaggar BL, Lessov-Schlaggar CN, Petersen SE (2013): Evidence for hubs in human functional brain networks. Neuron 79:798–813.

Rack-Gomer AL, Liu TT (2012): Caffeine increases the temporal variability of resting-state BOLD connectivity in the motor cortex. Neuroimage 59:2994–3002.

Rushworth MFS, Behrens TEJ, Johansen-Berg H (2006): Connection patterns distinguish 3 regions of human parietal cortex. Cereb Cortex 16:1418–1430.

Saad ZS, Gotts SJ, Murphy K, Chen G, Jo HJ, Martin A, Cox RW (2012): Trouble at rest: How correlation patterns and group

differences become distorted after global signal regression. Brain Connect 2:25–32.

Shen X, Papademetris X, Constable RT (2010): Graph-theory based parcellation of functional subunits in the brain from resting-state fMRI data. Neuroimage 50:1027–1035.

Shen X, Tokoglu F, Papademetris X, Constable RT (2013): Group-wise whole-brain parcellation from resting-state fMRI data for network node identification. Neuroimage 82C:403–415.

Smith SM, Fox PT, Miller KL, Glahn DC, Fox PM, Mackay CE, Filippini N, Watkins KE, Toro R, Laird AR, Beckmann CF. (2009): Correspondence of the brain's functional architecture during activation and rest. Proc Natl Acad Sci USA 106:13040–13045.

Szczepanski SM, Pinsk MA, Douglas MM, Kastner S, Saalmann YB (2013): Functional and structural architecture of the human dorsal frontoparietal attention network. Proc Natl Acad Sci USA 110:15806–15811.

Tagliazucchi E, Balenzuela P, Fraiman D, Chialvo DR (2012): Criticality in large-scale brain FMRI dynamics unveiled by a novel point process analysis. Front Physiol 3:15.

Tomasi D, Volkow ND (2011): Association between functional connectivity hubs and brain networks. Cereb Cortex 21:2003–2013.

Tomasi D, Volkow ND (2012): Resting functional connectivity of language networks: Characterization and reproducibility. Mol Psychiatry 17:841–854.

Tomasi D, Wang R, Wang GJ, Volkow ND (2013): Functional connectivity and brain activation: A synergistic approach. Cereb Cortex 24:2619–2629.

Toro R, Fox PT, Paus T (2008): Functional coactivation map of the human brain. Cereb Cortex 18:2553–2559.

van den Heuvel MP, Mandl RC, Kahn RS, Hulshoff Pol HE (2009): Functionally linked resting-state networks reflect the underlying structural connectivity architecture of the human brain. Hum Brain Mapp 30:3127–3141.

Van Dijk KR, Hedden T, Venkataraman A, Evans KC, Lazar SW, Buckner RL (2010): Intrinsic functional connectivity as a tool for human connectomics: Theory, properties, and optimization. J Neurophysiol 103:297–321.

Wang Y, Li TQ (2013): Analysis of whole-brain resting-state FMRI data using hierarchical clustering approach. PLoS One 8: e76315.

Weissenbacher A, Kasess C, Gerstl F, Lanzenberger R, Moser E, Windischberger C (2009): Correlations and anticorrelations in resting-state functional connectivity MRI: A quantitative comparison of preprocessing strategies. Neuroimage 47:1408–1416.

Windischberger C, Langenberger H, Sycha T, Tschernko EM, Fuchsjäger-Mayerl G, Schmetterer L, Moser E (2002): On the origin of respiratory artifacts in BOLD-EPI of the human brain. Magn Reson Imaging 20:575–582.

Yeo BT, Krienen FM, Sepulcre J, Sabuncu MR, Lashkari D, Hollinshead M, Roffman JL, Smoller JW, Zöllei L, Polimeni JR, Fischl B, Liu H, Buckner RL. (2011): The organization of the human cerebral cortex estimated by intrinsic functional connectivity. J Neurophysiol 106:1125–1165.

Young L, Dodell-Feder D, Saxe R (2010): What gets the attention of the temporo-parietal junction? An fMRI investigation of attention and theory of mind. Neuropsychologia 48:2658–2664.